ISSN 0030-400X, Optics and Spectroscopy, 2019, Vol. 126, No. 2, pp. 111–117. © Pleiades Publishing, Ltd., 2019.
Russian Text © I.V. Stanishevsky, T.A. Pavich, S.M. Arabei, 2019, published in Optika i Spektroskopiya, 2019, Vol. 126, No. 2, pp. 134–140.

SPECTROSCOPY OF CONDENSED STATE

A Study of the Ligand Composition Change of the Eu^{3+} Chelate by Two-Stage Laser Excitation Luminescence and Computer Simulation of Kinetics

I. V. Stanishevsky[a, *], T. A. Pavich[b], and S. M. Arabei[a]

[a] *Belarusian State Agrarian Technical University, Minsk, 220023 Belarus*
[b] *Stepanov Institute of Physics, National Academy of Sciences of Belarus, Minsk, 220072 Belarus*
**e-mail: ivanstanisheuski@mail.ru*

Received June 11, 2018

Abstract—The europium(III)–tris(dibenzoylmethane)–triphenylphosphine oxide complex was studied in the polycrystalline state and in toluene at 298 K using the luminescence excitation method with two-stage rectangular pulses with decreasing intensity of stages. Experimental nonmonotonic kinetic curves were numerically simulated within the framework of a four-level dynamic model describing reversible processes in the complex, associated with its structural rearrangement. The maximum correspondence between the experimental and simulated curves was obtained using an iterative approximation performed using the Nelder–Mead algorithm. Based on the obtained numerical values of the rate constants and parameters of the model, experimental kinetics were interpreted, and it was concluded that they are a consequence of the processes associated with changes in the ligand composition of the Eu^{3+} chelate.

DOI: 10.1134/S0030400X1902022X

INTRODUCTION

Among the complex compounds most popular for practical applications, lanthanide (Ln) chelates with organic ligands occupy a special place. This is mainly due to the high luminescence quantum yield of Ln^{3+} ions, the millisecond range of the lifetime of radiative states, the large Stokes shift, and the fixed position of narrow bands of electronic transitions. The complexes are successfully used to create new active laser media and polymer fiber amplifiers for the purposes of optical communications [1]. Considerable advances have been achieved in the development of electroluminescent materials based on them: organic light-emitting diodes [2], color displays and solid-state micro sources of white light [3], light-transforming coatings for solar cells [4], and luminescence sensors [5]. These complexes have shown promise in biological and medical developments [6], in studying biological processes in vitro and in vivo [7], as luminescent probes for diagnosing malignant tumors [8], and in immunological examinations [9].

The quantum yield of the sensitized luminescence of the complexes is mainly controlled by nonradiative deactivation of energy from the charge transfer state (CTS). The quantum yield value depends on the energy position of the CTS with respect to the levels of ligands and the lanthanide ion [10, 11] and on temperature [12, 13]. However, the quantum yield can decrease significantly when water molecules in the form of additional ligands enter the internal coordination sphere of the Ln^{3+} ion [14, 15]. In this case, quenching is due to nonradiative deactivation of excited states of the Ln^{3+} ion by high-frequency overtones of the valence O–H vibrations of water molecules [16].

For lanthanoid complexes in the polycrystalline state and in solution, the number of coordination sites occupied by ligands in the inner sphere (coordination number) can vary from 6 to 12. In the case of coordination unsaturation to Ln^{3+}, water molecules can be coordinated from the local environment. At the same time, in some solutions under dark conditions and during photoexcitation (PE), a number of complexes undergo a complex steric reorganization of the internal and/or external coordination spheres. This leads to a change in their ligand composition (first of all, the number of water molecules) and, as a result, to a change in the spectral-kinetic parameters of the luminescence. For example, the enhancement in the luminescence of Ln^{3+} tris-β-diketonates in toluene was detected after adding water to the solution [17]. The authors interpreted the unexpected effect by the formation of outer-sphere water associates, leading to the dissociation of weakly luminescent dimeric complexes, as well as a decrease in nonradiative losses through CTS. A similar effect for Eu^{3+} β-diketonate

complexes was observed in porous glass [18]. In the latter case, the inclusion of water molecules into the outer coordination sphere of the complex enhanced the $\pi \rightarrow \pi^*$ transitions in the conjugated ligand system, thereby increasing the population efficiency of the $^5D_0$ state. Bünzli and Piguet [19] described an analytical sensor for detecting and quantifying substances, the principle of which is based on enhancing the lanthanoid complex luminescence as a result of the release of water molecules from the internal coordination sphere during the photoexcitation of the complex and their replacement by analyte molecules. The increase in the luminescence quantum yield was associated with the ability of some organic solvents to displace water from the internal coordination sphere of the Ln^{3+} complexes [15, 20]. For example, the ligand exchange rates were determined by analyzing the luminescence decay kinetics of labile complexes in liquid solutions under pulsed selective laser excitation [15]. For the successful application of the method, it was necessary that the ligand exchange rate significantly exceeded the deactivation rate of the excited states of the Ln^{3+} ions. The works noted above indicate that the nature and composition of the ligand environment of Ln^{3+} ions significantly affect the parameters of their luminescence. There are all resons to assume that if an adequate kinetic model of the process is selected (including a ligand exchange one), its parameters can be determined. We have successfully applied the newly developed methods for studying the kinetics of photoprocesses to obtain information on the intramolecular rate constants and the ligand exchange rates. For example, a method for characterizing the metastable electronic states of organic molecules, based on the analysis of the decrease and increase of the fluorescence intensity kinetics excited by an amplitude-modulated quasi-stationary laser was described in [21, 22]. In addition to the simulation of the dynamics of the observed photoprocesses, an iterative approximation of the complex nonmonotonic luminescence kinetics profile was firstly implemented in [23]. An essential feature of the method is that it enables one to detect and characterize quantitatively all the photoprocesses occurring in the submillisecond and longer time ranges, including those associated with changes in the ligand composition in the lanthanoid complexes. The methods make it possible to study relatively slow changes in the physico-chemical and structural properties (photo durability, aging, etc.) of objects. Such information for the Eu^{3+} complex is difficult to obtain in the case of both stationary and typical pulsed (laser) photoexcitation.

The purpose of this work was to study the kinetics of the luminescence of the Eu^{3+} complex using amplitude modulated laser excitation and computer simulation to obtain information on the ligand exchange rates, based on which one can judge the qualitative composition of the ligand environment of the Eu^{3+} ion in the internal coordination sphere.

EXPERIMENTAL

A europium(III)–tris(dibenzoylmethane)–triphenylphosphine oxide complex ($Eu(DBM)_3TPPO$) was studied, where DBM is dibenzoylmethane and TPPO is triphenylphosphine oxide; the structure of the complex is shown in Fig. 1. The complex was synthesized according to a modified procedure [24] from the following components: europium nitrate ($Eu(NO_3)_3 \cdot 6H_2O$), DBM, and TPPO at a molar ratio of 1 : 3 : 1. DBM and TPPO compounds were dissolved in ethanol and, under vigorous stirring, added dropwise to the 1*N* aqueous solution of NaOH, adjusting the pH to 6.0. An aqueous solution of europium nitrate was added dropwise to the resulting solution. The reaction mixture was evaporated, and the precipitate of $Eu(DBM)_3TPPO$ was filtered, washed with a mixture of water and ethanol in the 1 : 1 ratio, dried to constant weight in a desiccator over anhydrous calcium chloride, and then recrystallized in acetone.

The luminescence of the complex was studied in a solid polycrystalline finely dispersed state (hereinafter, in a polycrystal) and in a solution (toluene) at 298 K. Modulated radiation of a semiconductor laser diode (λ_{gen} = 405 nm) was used for the excitation, the profile of which consisted of rectangular, decreasing in intensity two-stage pulses. The main details of the measurements were described in [21, 22]. In this work, the technique was improved: the photoexcitation profile, which was taken into account in the calculations, was recorded by measuring the luminescence kinetics of Rhodamine B in ethanol. The stationary absorption spectrum of the complex in solution at 298 K was measured using a Cary-500 Scan UV-Vis-NIR spectrophotometer (Varian, United States, Australia).

The interpretation of empirical data was based on the results of a numerical simulation using the following techniques and methods. First, the characteristic rates of the processes were found for the monotonic parts of the experimental curves, using the inverse problem algorithms [25, 26]. Further, the dynamics of populations of energy levels were calculated numerically, and the luminescence was simulated on the basis of the chosen one-dimensional kinetic model of reversible photoprocesses, described by the system of ordinary differential equations (SODE). The models did not take into account stimulated emission, intermolecular interactions, and irreversible photoprocesses. In this case, some initial values of the SODE coefficients were set taking into account the characteristic rates of the processes obtained earlier. The calculations were discussed in [21–23, 27] in more details. The numerical integration methods were used because the models with more than three levels did not have an exact analytical solution. In addition to direct calcula-

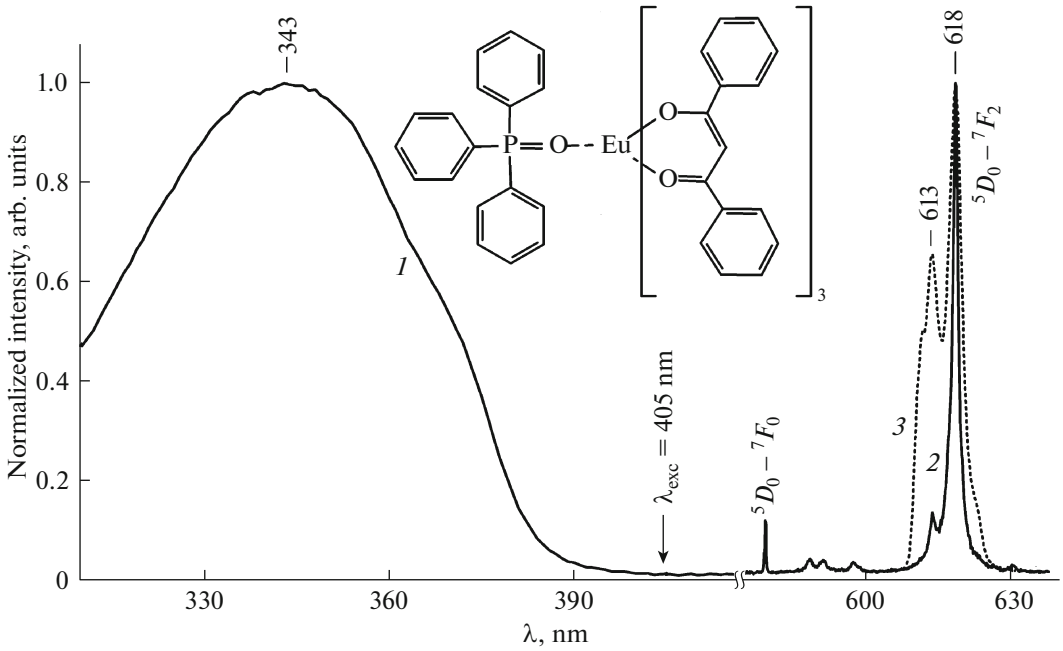

Fig. 1. (*1*) Normalized absorption spectra of $Eu(DBM)_3TPPO$ in toluene and luminescence spectra (*2*) in polycrystal and (*3*) in toluene at λ_{exc} = 405 nm and 298 K. Inset: chemical structure of $Eu(DBM)_3TPPO$.

tions of populations, an iterative approximation of experimental nonmonotonic kinetic curves by simulated luminescence curves was performed to determine the model parameters and rate constants of intramolecular and intermolecular processes. This inverse problem was solved using the Nelder–Mead optimization algorithm [28], which does not use derivatives when searching for the solution. As in [23], the objective function was minimized iteratively, which was the sum of squared intensity differences at given time points: the numerical values of the simulated luminescence curve and the corresponding values of the experimental curve. It should be emphasized that, in contrast to the widely used fit methods of monotonic parts of experimental curves by exponential functions, this paper presents the results of the approximation of nonmonotonic curves by superposition of SODE solutions over their entire time range. For the tested hypothetical models, the coefficients (rate constants) of SODE and parameters were varied, and a new optimal solution was found. The number of variable rate constants and model parameters was limited to a minimum sufficient number (no more than 8) to increase the reliability and uniqueness of the solution. The criterion for the final selection of the model was as follows. The model should ensure (1) the minimum value of the objective function, (2) the detailed correspondence of the profiles of the matched kinetic curves, and most importantly, (3) the physically plausible values of the calculated rate constants. All calculations were performed using the original procedures created by the authors, written and implemented in the Scilab environment [29]. The computational part of the procedures contained both the plug-in modules of the known libraries [25, 26] and the Scilab built-in modules (in particular, *neldermead_new*).

RESULTS AND DISCUSSION

The absorption spectrum of $Eu(DBM)_3TPPO$ in the region of 310–415 nm is shown in Fig. 1 (curve *1*). An intense broad band with a maximum at 343 nm, corresponding to the $S_0 \rightarrow S_1$ transitions of organic ligands is observed.

The luminescence of the Eu^{3+} ion is manifested due to the efficient intercombination conversion of $S_1 \rightsquigarrow T_1$ inside the ligand and the energy transfer from the T_1 level to the emitting $^5D_0$ level of Eu^{3+}. The luminescence spectrum of a polycrystal (Fig. 1, curve *2*) has rather narrow bands within 575–640 nm corresponding to the $^5D_0 \rightarrow {}^7F_i$ transitions, where $i = 0–2$. The most intense of them (610–620 nm) belongs to the $^5D_0 \rightarrow {}^7F_2$ transition, which is most sensitive to the symmetry of the nearest environment of Eu^{3+}. At room temperature in a toluene solution, this band consists of several intense components (Fig. 1, curve *3*), which indicates the low symmetry of the complex. We note that a single line at 580 nm (transition $^5D_0 \rightarrow {}^7F_0$) proofs the purity of the explored complex.

The luminescence kinetics has a specific behavior, that is, the profile of the experimental curves differs

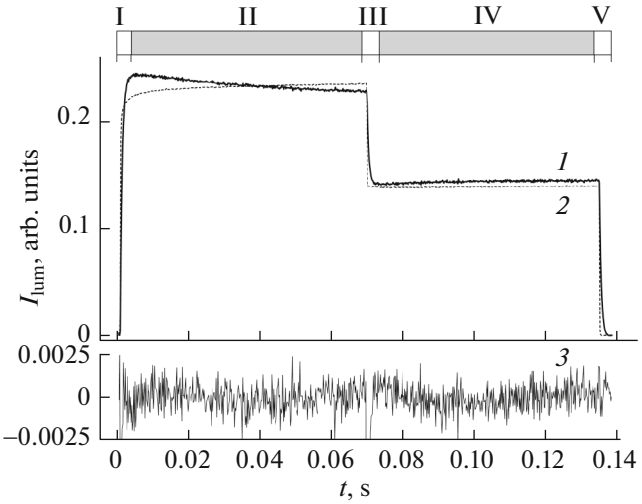

Fig. 2. (*1*) Luminescence kinetic curve of $Eu(DBM)_3TPPO$ in a polycrystal at 298 K (λ_{exc} = 405 nm, λ_{mon} = 618 nm, $\Delta\lambda_{mon} \approx 0.2$ nm). (*2*) Profile of the photoexcitation laser pulse. (*3*) Difference between the experimental and calculated luminescence intensities.

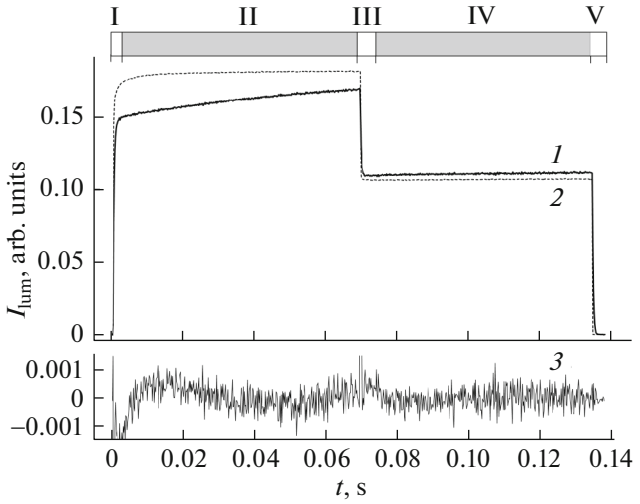

Fig. 3. (*1*) Luminescence kinetic curve of $Eu(DBM)_3TPPO$ in toluene at 298 K (λ_{exc} = 405 nm, λ_{mon} = 612 nm, $\Delta\lambda_{mon} \approx 1.0$ nm). (*2*) Profile of the photoexcitation laser pulse. (*3*) Difference between the experimental and calculated luminescence intensities.

remarkably from the profile of the photoexcitation pulse. In particular, for a polycrystal, the kinetics has the profile shown in Fig. 2 (curve *1*) when recording within the contour of the 610–620 nm band. In toluene, a similar kinetic profile is observed only at λ_{mon} = 618 nm, and when shifted to the shortwave region (λ_{mon} = 612 nm), it smoothly transforms into the profile shown in Fig. 3 (curve *1*). If the kinetic curve is conditionally divided into parts, which in Figs. 2 and 3 are indicated as I–V, then the most significant differences are observed in parts II and IV, corresponding to each individual stage of photoexcitation. For a polycrystal, the intensity decreases in part II and increases in part IV. In toluene, the opposite picture is observed, in particular, at λ_{mon} = 612 nm. Typical rates of intensity change in parts I, III, and V are ~2000 s^{-1} for polycrystal and ~4500 s^{-1} for toluene, and in parts II and IV, they are, respectively, ~30 and ~10 s^{-1}. For all the parts, the dispersion of the rate constant values of the processes (nonmonoexponentiality of the curves) was revealed.

The generally accepted cascade mechanism for the migration of the photoexcitation energy in organic lanthanide complexes, when after the intercombination conversion from the excited singlet level S_1 to the triplet level T_1 of the ligand, energy is transferred to the $^5D_1$ level of Eu^{3+} and further to its radiative $^5D_0$ level, is unable to explain the observed kinetics in parts II and IV. Taking into account the well-known typical the rate constant values of the intracomplex population processes of the Eu^{3+} levels (>10^6 s^{-1}) [13, 30], it can be argued that the cascade process of the photoexcitation energy migration in the Eu^{3+} complex can be quite correctly simplified by an equivalent one-stage process. For example, the process, in which the $^5D_0$ level is directly populated under photoexcitation, which is then deactivated to ^7F_i levels. Typical values of the rate of intensity change in parts I, III, and V were expectedly close to the known rate constants of the $^5D_0 \rightarrow {}^7F_2$ transition (≈2000–4000 s^{-1}) [13, 30]. However, the rates in parts II and IV were two orders of magnitude lower. The question arises as follows which slow (0–1000 s^{-1}) molecular processes determine this behavior of the curves in these parts. It can be argued that the energy levels participating in the migration of photoexcitation energy to the Eu^{3+} ion cannot be involved in such slow processes. This is because the deactivation rate constants of these levels (including the CTS level) exceed 10^6 s^{-1}, which is significantly higher than the observed maximum rates (4000 s^{-1}) of the intensity change. The participation of the phonons of the crystal lattice [13] in slow processes is all the more impossible since, at 298 K, they have picosecond characteristic lifetimes.

It is important to note that the observed decrease and increase in luminescence, in particular, in a polycrystal, has a noticeable similarity to the kinetics of fading and antifading of the porphyrin fluorescence [21, 22]. The effects in the latter were associated with the processes of reaching different equilibrium populations of the metastable T_1 state with the two-stage photoexcitation intensity change. The calculations performed in [23] showed that this similarity is caused by reversible structural phototransformations of the Eu^{3+} complex, which also lead to a change in the equilibrium populations of its energy levels. Based on test-

ing three- and four-level models, the one that most adequately described the experimental kinetic dependences for both the polycrystal and the solution according to the above mentioned criteria was chosen. The model included transitions in and between two two-level complexes K1 and K2, which are assumed additionally related to each other by reversible transformations. In the case of $Eu(DBM)_3TPPO$, such transformations can be reversible structural photoconversions. The diagram of energy levels and transitions between them for the speculated model is shown in Fig. 4.

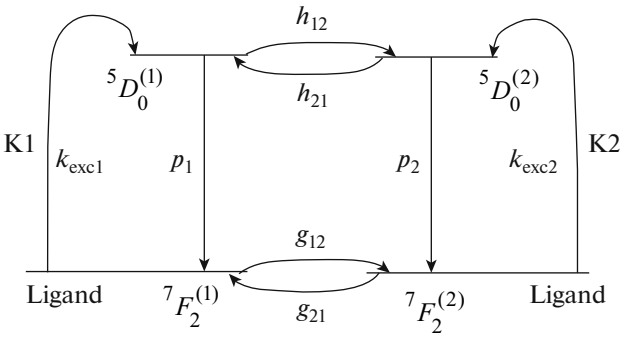

Fig. 4. Energy levels of the K1 and K2 complexes and transitions between them: k_{exc1} and k_{exc2} are the rate constants of photoexcitation; p_1 and p_2 are the total rate constants of the intramolecular deactivation of the levels $^5D_0^{(1)}$ and $^5D_0^{(2)}$; h_{12} and h_{21} are the rate constants of the direct and reverse phototransformations in the $^5D_0^{(1)}$ and $^5D_0^{(2)}$ states; and g_{12} and g_{21} are the rate constants of the direct and reverse dark transformations in the $^7F_2^{(1)}$ and $^7F_2^{(2)}$ states.

The population path of the $^5D_0^{(1)}$ and $^5D_0^{(2)}$ levels of the K1 and K2 complexes as a result of the fast cascade migration of the photoexcitation energy from the ligand to Eu^{3+} is shown in the diagram as curved arrows and turned out to be quite an acceptable simplification. In order to decrease the number of SODE coefficients, it was assumed that transitions between K1 and K2 took place only between the excited levels $^5D_0^{(1)}$ and $^5D_0^{(2)}$ (the corresponding transition rate constants are h_{12} and h_{21}) and the ground levels $^7F_2^{(1)}$ and $^7F_2^{(2)}$ (g_{12} and g_{21}). The SODE describing the model had the form of

$$\begin{cases} [b]\dfrac{d[^7F_2^{(1)}]}{dt} = -(k_{exc1}+g_{12})[^7F_2^{(1)}] + p_1[^5D_0^{(1)}] + g_{21}[^7F_2^{(2)}], \\ \dfrac{d[^5D_0^{(1)}]}{dt} = -(p_1+h_{12})[^5D_0^{(1)}] + k_{exc1}[^7F_2^{(1)}] + h_{12}[^5D_0^{(2)}], \\ \dfrac{d[^7F_2^{(2)}]}{dt} = -(k_{exc2}+g_{21})[^7F_2^{(2)}] + p_2[^5D_0^{(2)}] + g_{12}[^7F_2^{(1)}], \\ \dfrac{d[^5D_0^{(2)}]}{dt} = -(p_2+h_{21})[^5D_0^{(2)}] + k_{exc2}[^7F_2^{(2)}] + h_{12}[^5D_0^{(1)}]. \end{cases} \quad (1)$$

The system (1) was assumed to be closed: $[^7F_2^{(1)}(t)] + [^7F_2^{(2)}(t)] + [^5D_0^{(1)}(t)] + [^5D_0^{(2)}(t)] = [^7F_2^{(1)}(0)] + [^7F_2^{(2)}(0)] = n_1 + n_2 = \text{const}$. The parameters n_1 and n_2 were the initial concentrations of the K1 and K2 complexes, respectively. The luminescence intensity was calculated as the sum of the populations of the excited $^5D_0^{(1)}$ and $^5D_0^{(2)}$ levels with their weight contributions r_1 and r_2: $I(t)_{lum} \sim r_1[^5D_0^{(1)}(t)] + r_2[^5D_0^{(2)}(t)]$. Parameters r_1 and r_2 were essentially radiative contributions to p_1 and p_2, respectively. Table 1 shows the calculated values of the transition rate constants and parameters of the considered model.

Analysis of the calculated data for $Eu(DBM)_3TPPO$ in a polycrystal shows that in the ground state, it exists mainly in the form of the K1 complex ($n_1 > n_2$), but its excitation efficiency is low ($k_{exc1} \ll k_{exc2}$). In the $^5D_0^{(1)}$ state, K1 is converted to K2 with an efficiency of $\sim 0.05(h_{12}/(p_1 + h_{12}))$ due to the $^5D_0^{(1)} \rightsquigarrow {}^5D_0^{(2)}$ transition. The back process $^5D_0^{(1)} \leftsquigarrow {}^5D_0^{(2)}$ is less efficient ($h_{12} > h_{21}$). The relations of $p_1 > p_2$ and $r_1 < r_2$ are valid. In the ground state, the equilibrium between the reversible dark processes of the K1 $\leftrightsquigarrow$ K2 transformations is shifted towards the formation of K1 ($g_{12} < g_{21}$). Note that the formation rate of K2 in the excited state exceeds its decay rate in the ground state ($h_{12} \gg g_{21}$). The time parameters of the luminescence kinetics in parts I, III, and V are well correlated with the values of p_1 and p_2, and in parts II and IV, they have the same order of magnitude as the calculated values of h_{12}, h_{21}, g_{12}, and g_{21}. These rate constants determine the observed slow intensity changes. Calculations showed that the decrease and increase of the luminescence intensity in parts II and IV are caused both by the accumulation of molecules at the ground level of K2 ($^7F_2^{(2)}$) and are the result of a change in the populations of all energy levels of K1 and K2. The latter differs from the case of porphyrins [21, 22].

In toluene, the values of n_2, r_1, r_2, and also h_{12}, h_{21}, g_{12}, and g_{21} are smaller than those in polycrystal; although, the proportionality is observed between the same constants. In this case, the values of p_1 and p_2 are higher than the corresponding values in the polycrystal. As in the case of a polycrystal, slow changes in the luminescence intensity are a result of both a change in the populations of all levels and the formation of long-lived K2. However, the lower values of h_{12}, h_{21}, g_{12}, and, most importantly, g_{21} lead to the fact that in parts II and IV, an increase in the luminescence intensity is observed (Fig. 3). Calculations of the kinetics at $\lambda_{mon} = 618$ nm (in this case, as was noted, the kinetics

Table 1. Calculated values of the rate constants and parameters of the model

Parameters and rate constants	Polycrystal (λ_{mon} = 618 nm)		Solution (λ_{mon} = 612 nm)	
	parameter, arb. units	rate constant, s^{-1}	parameter, arb. units	rate constant, s^{-1}
n_1	1	–	1	–
n_2	0.2–0.5	–	0.05–0.1	–
r_1	0.01–0.1	–	0.02–0.05	–
r_2	0.3–0.5	–	0.05–0.1	–
k_{exc1}	–	3–10	–	200–400
k_{exc2}	–	300–1000	–	2000–4000
p_1	–	2500–4500	–	5200–6000
p_2	–	1900–2200	–	3200–3800
h_{12}	–	80–250	–	20–30
h_{21}	–	50–65	–	12–16
g_{12}	–	3–7	–	0.1–0.3
g_{21}	–	16–20	–	3–8

profile is similar to that observed in a polycrystal) proved that some of these constants increase noticeably.

The computations suggest the following qualitative picture of the physical processes in $Eu(DBM)_3TPPO$. The values of the total rate constants p_1 and p_2 and their relation ($p_1 > p_2$), as well as the relation of the parameters r_1 and r_2 ($r_1 < r_2$), allow to assume, taking into account the data of [14, 15], that the first coordination sphere of the K1 complex contains quencher molecules (water), whereas there are no quenchers in the first coordination sphere of the K2 complex, or they are fewer than in K1. The water molecules, being in the first coordination sphere of K1 in the form of n additional ligands ($[Eu(DBM)_3TPPO(H_2O)_n]$, participate in the nonradiative exchange of the excitation energy of the Eu^{3+} ion to the energy of the own overtones of high-frequency O–H vibrations, which is confirmed by small values of r_1. In the excited state, the strength of the Eu^{3+} bonds with the inner-sphere ligands weakens, and some (m) water molecules leave the internal coordination sphere, resulting in a more luminescent excited complex K2 $[Eu(DBM)_3TPPO(H_2O)_{n-m}]^* \cdot (H_2O)_m$. A decrease in the number of water molecules within the first coordination sphere leads to a decrease in the total rate constant p_2 with a simultaneous increase in the luminescence intensity (due to an increase in r_2). In the ground state of K2, $[Eu(DBM)_3TPPO(H_2O)_{n-m}] \cdot (H_2O)_m$, labile water molecules that left the coordination sphere are again bound to Eu^{3+}, with the result that the original ligand environment in the inner sphere is restored, and K2 is transformed into K1, $[Eu(DBM)_3TPPO(H_2O)_n]$. Thus, the general mechanism of reversible transformations of K1 ⇜⇝ K2 is as follows:

$$\begin{array}{ccc} [Eu(DBM)_3TPPO(H_2O)_n]^* & \underset{h_{21}}{\overset{h_{12}}{\rightleftharpoons}} & [Eu(DBM)_3TPPO(H_2O)_{n-m}]^*(H_2O)_m \\ \text{(K1)} \quad k_{exc1}\uparrow \quad \downarrow p_1 & & k_{exc2}\uparrow \quad \downarrow p_2 \quad \text{(K2)} \\ [Eu(DBM)_3TPPO(H_2O)_n] & \underset{g_{21}}{\overset{g_{12}}{\rightleftharpoons}} & [Eu(DBM)_3TPPO(H_2O)_{n-m}](H_2O)_m \end{array}$$

A weighty argument in favor of the described mechanism of transformations is the fact that at 77 K, the intensity of the luminescence in parts II and IV completely repeats the photoexcitation profile. It is evident that at a low temperature, water molecules are not labile, and the ligand composition of the complex remains unchanged.

For the solution, there may be an alternative interpretation of the results, similar to that given in [17]. The K1 complexes, being in the environment of hydrophobic toluene, form outer-sphere associates that do not luminesce. Under the action of photoexcitation, the water molecules leave the first coordination sphere of the K1 complex, the associates decompose, and the luminescent complexes K2 form. Another

alternative interpretation is as follows: the movement of water molecules into the outer coordination sphere of the complex may enhance the $\pi \rightarrow \pi^*$ transitions in ligands [18] and thus increase the emission from the $^5D_0^{(2)}$ level by increasing r_2.

CONCLUSIONS

The method of generating rectangular two-stage laser pulses with decreasing intensity, applied to the study of reversible photoprocesses in the Eu^{3+} chelate, gave information that is difficult or impossible to obtain using other methods of optical spectroscopy. A computer simulation of the nonmonotonic luminescence kinetics of Eu^{3+}, performed using a numerical solution of a system of ordinary differential (kinetic) equations describing the processes in the selected model, was supplemented with an iterative approximation of non-monotonous solutions. This simulation was implemented using the Nelder–Mead algorithm, which does not use derivatives. It enabled not only to achieve the maximum fit (similarity) of the experimental and simulated curves compared but also to obtain the numerical values of the rate constants and parameters of the model. This approach for analyzing the kinetics was applied, apparently, for the first time (in spectroscopic data treatment), and despite the significantly increased amounts of computation, it grounded quantitatively the interpretation of the data obtained. The calculated numerical values of the rate constants and parameters of the model allowed to conclude that in $Eu(DBM)_3TPPO$, there is a change in the ligand composition in the ground and excited states. The latter is a type of hydration isomerism, in which the redistribution of water molecules takes place between the internal and external coordination spheres at photoexcitation. It should be noted that an alternative interpretation is possible for the solution of the complex.

ACKNOWLEDGMENTS

This work was partially supported by the Belarusian Republican Foundation for Fundamental Research, project no. F17-005.

REFERENCES

1. K. Kuriki, Y. Koike, and Y. Okamoto, Chem. Rev. **102**, 2347 (2002).
2. J. Kido and Y. Okamoto, Chem. Rev. **102**, 2357 (2002).
3. G. F. de Sá, O. L. Malta, C. de Mello Donegá, A. M. Simas, R. L. Longo, P. A. Santa-Cruz, and E. F. da Silva, Jr., Coord. Chem. Rev. **196**, 165 (2000).
4. T. Fukuda, S. Kato, E. Kin, K. Okaniwa, H. Morikawa, Z. Honda, and N. Kamata, Opt. Mater. **32**, 22 (2009).
5. H. Tsukube and S. Shinoda, Chem. Rev. **102**, 2389 (2002).
6. S. V. Eliseeva and J.-C. G. Bünzli, Chem. Soc. Rev. **39** (18), 189 (2010).
7. V. V. Zherdeva and A. P. Savitskii, Usp. Biol. Khim. **52**, 315 (2012).
8. T. A. Pavich, A. V. Vorobey, S. M. Arabei, and K. N. Solovyov, J. Appl. Spectrosc. **79**, 651 (2012).
9. T. Lovgren and K. Pettersson, in *Luminescence Immunoassay and Molecular Application,* Ed. by K. van Dyke and R. van Dyke (CRC, Boca Raton, FL, 1990).
10. M. Latva, H. Takalo, V.-M. Mukkala, C. Matachescu, J. C. Rodriguez-Ubis, and J. Kankare, J. Lumin. **75**, 149 (1997).
11. W. M. Faustino, O. L. Malta, and G. F. de Sá, J. Chem. Phys. **122**, 054109 (2005).
12. M. T. Berry, P. S. May, and H. Xu, Phys. Chem. **100**, 9216 (1996).
13. V. Ya. Venchikov and M. P. Tsvirko, J. Appl. Spectrosc. **68**, 473 (2001).
14. F. S. Richardson, Chem. Rev. **82**, 541 (1982).
15. V. L. Ermolaev and E. B. Sveshnikova, Russ. Chem. Rev. **63**, 905 (1994).
16. A. Beeby, I. M. Clarkson, R. S. Dickins, S. Faulkner, D. Parker, L. Royle, A. S. de Sousa, J. A. Gareth Williams, and M. Woods, J. Chem. Soc., Perkin Trans. 2, 493 (1999).
17. A. I. Voloshin, N. M. Shavaleev, and V. P. Kazakov, J. Photochem. Photobiol., A **136**, 203 (2000).
18. A. A. Petushkov, S. M. Shilov, M. V. Puzyk, and V. N. Pak, Tech. Phys. Lett. **32**, 399 (2006).
19. J.-C. G. Bünzli and C. Piguet, Chem. Soc. Rev. **34**, 1048 (2005).
20. Yu. V. Korovin, N. V. Rusakova, and S. B. Meshkova, Ukr. Khim. Zh. **66** (10), 121 (2000).
21. I. V. Stanishevsky, K. N. Solov'ev, S. M. Arabei, and V. A. Chernyavskii, J. Appl. Spectrosc. **80**, 357 (2013).
22. I. V. Stanishevsky, S. M. Arabei, V. A. Chernyavskii, and K. N. Solovyev, Opt. Spectrosc. **121**, 722 (2016).
23. I. V. Stanishevsky, S. M. Arabei, and T. A. Pavich, in *Proceedings of the 11th International Conference on Quantum Electronics* (RIVSh, Minsk, 2017), p. 39.
24. W. Hu, M. Matsumura, M. Wang, and L. Jin, Jpn. J. Appl. Phys. **39**, 6445 (2000).
25. S. W. Provencher, Comput. Phys. Commun. **27**, 213 (1982).
26. C. Elster, J. Honerkamp, and J. Weese, Rheol. Acta **31**, 161 (1992).
27. I. V. Stanishevsky and V. A. Chernyavskii, J. Appl. Spectrosc. **82**, 726 (2015).
28. J. A. Nelder and R. Mead, Comput. J. **7**, 308 (1965).
29. Scilab. https://en.wikipedia.org/wiki/Scilab.
30. S. Sato and M. Wada, Bul. Chem. Soc. Jpn. **43**, 1955 (1970).

Translated by O. Zhukova